Dynamic model for piezotronic and piezo-phototronic devices under low and high frequency external compressive stresses

Leisheng Jin[1], Xiaohong Yan[1], Xiangfu Wang[1], Weijun Hu[2], Yan Zhang[3], and Lijie Li[2*]

[1]School of Electronic Science and Engineering, Nanjing University of Posts and Telecommunications, China

[2]Multidisciplianary Nanotechnology Centre, College of Engineering, Swansea University, UK

[3]School of Physical Electronics, University of Electronic Science and Technology of China, Chengdu, China.

*Corresponding email: l.li@swansea.ac.uk

Abstract

In this work, we aim to establish a theoretical method for modelling dynamic characteristics of piezotronics and piezo-phototronic devices. By taking the simplest piezotronic device—PN junction as an example, we combine the small signal model and the unified approach to investigate its diffusion capacitance and conductance when it is under both low and high frequency external compressive stresses. This approach is different from the traditional considerations that treat the piezopotential as a static value. Furthermore, we expand the theory into piezo-phototronic devices e.g. a light emitting diode (LED). The dynamic recombination rate and light emitting intensity are quantitatively calculated under different frequencies of external compressive stresses.

Key Words: Piezotronics, Piezo-phototronics, Dynamics, Diffusion capacitance, Recombination rate

1. Introduction

Two emerging physical effects namely piezotronics and piezo-phototronics have been rapidly developed in recent years [1]. From the invention of single ZnO (zinc oxide) nanowire generator [2] to the demonstration of piezoelectricity in single-layer MoS_2 [3], from the observation of the coupling between piezoelectricity and photoexcitation in ZnO nanowires [4] to the successful applications of using piezopotential in active optoelectronics, such as luminescence devices for adaptive sensing [5], LEDs array for pressure imaging [6], photodetectors [7 8 9], solar cells [10, 11], and energy conversion [12], these two phenomena have been evolving toward more attractive research fields, bringing great potential in the development of wearable electronics, robotics, the IOT (internet of things), biomedical engineering and human–machine interfacing [13, 14 15 16]. The piezotronic effect of nanodevices has been thoroughly experimented using various

methodologies[17]. These achievements could not have been reached without understanding the fundamental physics behind the experimental observations. So far the theory of piezotronics and piezo-phototronics is based on the semi-analytical abrupt junction model [18]. The first principle simulations of piezotronic transistors have been conducted, which was based on the width changing of the piezoelectrically charged area [19]. In our previous work [20], a quantum scattering model was employed for investigating the ballistic carriers transportation in piezotronics. Meanwhile, numerical simulations using the DFT (density function theory) and FEM (finite element method) have also been conducted to investigate the device interfaces and carriers modulation on piezotronics [21] [22]. These theoretical developments have satisfactorily helped understand the existing experimental works [23] [24].

So far only the static characteristics of the devices have been simulated, in which the piezopotential was treated as a static value corresponding to a static compressive or tensile stress. In terms of dynamic investigation, models for piezotronics and piezo-phototronics have not been reported. The dynamic analysis for piezotronic and piezo-phototronic devices under a dynamic external force at a high frequency is usually essential in research and development of piezotronic and piezo-phototronic devices. For example in references [6] [23] , authors fabricated an array of LEDs to detect a dynamic pressure by emitting optical light based on the piezo-phototronic effect, where the impact of the frequency of the exerted pressure is important. Moreover, the quantitative dynamic effects due to the piezopotential on the carriers generation, recombination and transportation are not clear [25], although these terms are qualitatively used in explaining the experimental works [10, 26].

In this work, we develop a novel dynamic model for piezotronics and piezo-phototronics to investigate quantitatively how the dynamic stress affects the carriers generation and recombination processes, and to explore the dynamic light-emitting mechanism in piezo-phototronic LEDs. We use the most basic piezotronic device – a PN junction in the analysis, trying to construct a general model for peizotronic devices subject to dynamic external forces. External forces at both low and high frequencies are considered using a small-signal model together with the unified approach [27]. Furthermore, we calculate the dynamic recombination rate and light emitting rate in piezotronic and piezo-phototronic LEDs, providing a thorough understanding of the dynamic process of carriers under the piezopotential. The work complements existing theories for piezotronics and piezo-phototronics [18] [14].

2. Basic theory

Schematically shown in Figure 1, the structure studied here is a typical PN junction with the *n*-area made by ZnO. Due to the piezoelectricity of ZnO, piezoelectric charges will be accumulated at the two ends of the *n*-area of the PN junction when a compressed or tensile force is applied. The width of the distributed piezoelectric charges is denoted by W_{pz}, taking x=0 at the interface of *P* and *N* region. The PN junction is assumed to be metallurgical. The depletion widths on the *N* and *P* regions are represented by W_p and W_n, respectively. V_{dc} is the forward applied bias. First, we consider the case when V_{dc} is off and only a static compressive force is applied to one end of the *N* region. The electrical filed across the depletion region of the PN junction can be easily derived, which are given by following equations (1-3).

This manuscript was accepted by J. Appl. Phys. Click here to see the version of record.

$$E(x) = -\frac{eN_A(x+W_p)}{\varepsilon_s}, -W_p \le x \le 0 \quad (1)$$

$$E(x) = -\frac{e[N_D(W_n-x)+\rho_{pz}(W_{pz}-x)]}{\varepsilon_s}, 0 \le x \le W_{pz} \quad (2)$$

$$E(x) = -\frac{eN_D(W_n-x)}{\varepsilon_s}, W_p \le x \le W_n \quad (3)$$

where e is the elementary charge, N_A and N_D are donor and acceptor concentrations respectively. ε_s is the permittivity of the ZnO. ρ_{pz} is the density of polarization charges. The ρ_{pz} can be treated as one of the material properties, which is defined as number of piezoelectrically generated charges per unit volume. It is assumed as a constant for a given material representing the ability of accommodating piezoelectrically generated charges per unit volume. The density of polarization charges ρ_{pz} at the junction is positive when a compressive strain is applied and is negative when a tensile strain is applied. As the electrical field E is continuous at the metallurgical junction ($x=0$), by setting x=0 in equations (1) and (2), we have

$$N_A W_p = N_D W_n + \rho_{pz} W_{pz} \quad (4)$$

By integrating equations (1), (2) and (3), the potential $\varphi(x)$ in depletion regions [$-W_p$ 0], [0 W_p] and [W_p W_n] of the PN junction can be derived [18], and it is known as the built-in potential:

$$\varphi_{bi} = \frac{e}{2\varepsilon_s}(N_A W_p^2 + \rho_{pz} W_{pz}^2 + N_D W_n^2) \quad (5)$$

Combining equations (4) with (5), the built-in potential can be rewritten as:

$$\varphi_{bi} = \frac{e}{2\varepsilon_s}(N_A W_p^2 + \frac{N_A^2 W_p^2}{N_D} + \rho_{pz} W_{pz}^2 - \frac{2N_A W_p \rho_{pz} W_{pz}}{N_D} + \frac{\rho_{pz}^2 W_{pz}^2}{N_D}) \quad (6)$$

3. When time-variant compressive stress applied.

Now we assume there is a compressive stress varying as a sinusoidal function applied to the right end of ZnO, i.e. $F=F_0+F_1 sin(\omega t)$, where F_0 are F_1 represent amplitudes of the stress. ω is the frequency of the varying stress. W_p, ρ_{pz}, N_A, N_D are all considered to be constants during one period of the applied stress. When the applied stress is varying, the value of generated charges ($A_d \cdot \rho_{pz} \cdot W_{pz}$, A_d denotes the cross-sectional area, a constant for nanowire devices) varies. Hence W_{pz} varies in the same way as the external applied stress. Only W_{pz} is varying with the same frequency as F, the static built-in potential is then replaced by

$$\varphi_{bi}(t) = \frac{e}{2\varepsilon_s}\left(\left(N_A + \frac{N_A^2}{N_D}\right)W_p^2 + \left(\rho_{pz} + \frac{\rho_{pz}^2}{N_D}\right)\left(W_{pz0}^2 - 2W_{pz0}W_{pz1} sin\omega t + W_{pz1}^2 \sin^2\omega t\right) - \frac{2N_A W_p \rho_{pz}}{N_D}\left(W_{pz0} - W_{pz1} sin\omega t\right)\right) \quad (7)$$

where W_{pz0} is the width of piezoelectric charge region when only F_0 is added, and W_{pz1} is the width of piezoelectric charge region corresponding to F_1. The equation (7) can be rewritten to

$$\varphi_{bi}(t) = c_1 + c_2 - c_3 sin\omega t + c_4 \sin^2\omega t \quad (8)$$

by taking:

$$c_1 = \frac{e}{2\varepsilon_s}N_A W_p^2 + \frac{e}{2\varepsilon_s}\cdot\frac{N_A^2 W_p^2}{N_D};\ c_2 = \frac{e}{2\varepsilon_s}\left(\rho_{pz} + \frac{\rho_{pz}^2}{N_D}\right)W_{pz0}^2 - \frac{e}{2\varepsilon_s}\cdot\frac{2N_A W_p \rho_{pz}}{N_D}W_{pz0} \quad (9)$$

This manuscript was accepted by J. Appl. Phys. Click here to see the version of record.

$$c_3 = \frac{e}{2\varepsilon_s}\cdot\left(\rho_{pz}+\frac{\rho_{pz}^2}{N_D}\right)\cdot 2W_{pz0}W_{pz1} - \frac{e}{2\varepsilon_s}\cdot\frac{2N_A W_p \rho_{pz}}{N_D}\cdot W_{pz1};\ c_4 = \frac{e}{2\varepsilon_s}\left(\rho_{pz}+\frac{\rho_{pz}^2}{N_D}\right)W_{pz1}^2 \quad (10)$$

To have a clear picture of the dynamic built-in potential, we have calculated the φ_{bi} in Figure 2. The parameters are taken as: N_A=1x10^{16} cm^{-3}, N_D=1x10^{15} cm^{-3}, ε_s=8.91, W_{pz0}=2x10^{-7} cm and W_{pz1}=2x10^{-8} cm. In determining ρ_{pz} we have used the relation: $e_{33}s_{33}=e\rho_{pz}W_{pz0}$, in which e_{33}=1.22 C m^{-2} and s_{33}=0.05% [18 28]. The frequency of dynamical compressive force is taken as 1 KHz. From Figure 2, it is seen that the built-in potential varies with time with an approximate sinusoidal pattern. Moreover, we have shown the energy band changing under different compressive stains in Figure 3. The stains are changing from 0.002% to 0.1%, it is seen that the piezoelectric potential and the built-in potential ϕ_{bi} both increase accordingly. It should be noted that due to the change of piezoelectric potential, the width of depletion region also changes mainly from the change of *n*-region.

Based on the above results, we will consider the cases when the PN junction is forward biased and applied a varied compressive stress at the same time in the followed section. Admittance is the most important index in dynamic analysis of the PN junction. Therefore, we will study the small signal admittance brought by the varying piezoelectrical charges generated by the time-varying compressive stress *F*.

3.1 Low Frequency---small single model

Under the condition of thermal-equilibrium the relationship between minority carrier concentration in the *n*- part of the junction and majority carrier concentration on the *p*-side is given by:

$$p_{n0} = p_{p0}\exp\left(\frac{-e\varphi_{bi0}}{kT}\right) \quad (11)$$

where, φ_{bi0} is original built-in potential without applying any force and voltage, p_{n0} is hole concentration in *n*-side of the junction, p_{p0} is the hole concentration in *p*-side, *k* is Boltzmann constant and *T* is thermal temperature. When the V_{dc} is applied to the junction, the thermal-equilibrium is broken and the hole concentration in *n*-side becomes:

$$p_n = p_{p0}\exp\left(\frac{-e(\varphi_{bi0}-V_{dc})}{kT}\right) \quad (12)$$

Now consider the case when there is also a time varied compressive strains existing, we can write the p_n, as:

$$p_n = p_{p0}\exp\left(\frac{-e(c_1+c_2-c_3 sin\omega t+c_4\sin^2\omega t-V_{dc})}{kT}\right) \quad (13)$$

where we have taken equation (8) into consideration. The equation (13) can be further simplified as:

$$p_n(x=0) = p_{p0}\exp\left(\frac{e\left(V_{dc}'+v_1(t)-v_2(t)\right)}{kT}\right) = p_n(0,t) \quad (14)$$

where V_{dc}'=V$_{dc}$-c$_1$-c$_2$, $v_1(t)=c_3 sin\omega t$ and $v_2(t)=c_4 sin^2\omega t$. If we assume $V_{dc}'=V_{dc}''-\varphi_{bi0}$, the equation (14) can be rewritten as:

$$p_n(0,t) = p_{dc}''\exp\left(\frac{e(v_1(t)-v_2(t))}{kT}\right) \approx p_{dc}''\left(1+\frac{v_1(t)-v_2(t)}{V_t}\right) \quad (15)$$

where $p_{dc}''=p_{n0}exp(eV_{dc}''/kT)$, $kT/e=V_t$, equation (11) and Taylor expansion of the exponential term have been applied, and $|v_1(t)- v_2(t)|<<V_t$ have been assumed. Equation (15) will be taken as the boundary condition. Due to $c_4<<c_3$ in PN junction, the $v_2(t)$ will be ignored in the following analysis.

The electric field in the neutral *n* region is assumed to be zero. Thus, the behavior of the excess minority carriers (holes) that flow from *p* region can be described by:

$$D_p \frac{\partial^2(\delta p_n)}{\partial_x} - \frac{\delta p_n}{\tau_{p0}} = \frac{\partial \delta p_n}{\partial t} \tag{16}$$

Since the AC voltage that comes from the time-varying component of the built-in potential can be seen to superimpose on the DC level, we can write the $\delta p_n=\delta p_0(x)+p_1e^{jwt}$, where p_1 is magnitude of the AC component of the excess concentration. Substituting δp_n into equation (16), according to a standard small signal analysis for the PN junction, the DC component of the holes diffusion current density can be given by:

$$J_{p0} = \frac{eD_p p_{n0}}{L_p^2}\left[exp\left(\frac{eV_{dc}''}{kT}\right) - 1\right] \tag{17}$$

where $L_p^2=D_p\tau_{p0}$ and $C_p^2=(1+j\omega\tau_{p0})/ L_p^2$, τ_{p0} is the holes lifetime. This only represents the situation at x=0. The current density phasor for the sinusoidal component of the diffusion current density is given by:

$$\hat{J}_p = eD_pC_p\left[p_{dc}''\left(\frac{\hat{V}_1}{V_t}\right)\right]e^{-C_px}\Big|_{x=0} \tag{18}$$

The equation (18) can be further written as:

$$\hat{J}_p = J_{p0}\sqrt{1+j\omega\tau_{p0}}\left(\frac{\hat{V}_1}{V_t}\right) \tag{19}$$

where $J_{p0}=eD_pp_{dc}''$. Likewise, we can derive the current density phasor for minority carrier (electrons) in *p* region, which is given by:

$$\hat{J}_n = J_{n0}\sqrt{1+j\omega\tau_{p0}}\left(\frac{\hat{V}_1}{V_t}\right) \tag{20}$$

Combining equations (19) and (20), the PN junction admittance can be derived, that is

$$Y = \frac{A\hat{J}_p+A\hat{J}_n}{\hat{V}_1} = \left(\frac{1}{V_t}\right)\left[I_{p0}\sqrt{1+j\omega\tau_{p0}} + I_{n0}\sqrt{1+j\omega\tau_{n0}}\right] \tag{21}$$

If the AC signal induced by dynamic compressive stress is not large, i.e. $\omega\,\tau_{p0}<<1$ and $\omega\,\tau_{n0}<<1$ (ω is ignored as τ approximates to 10^{-7} s). The equation (21) can be written as: $Y=g_d+j\omega C_d$, where g_d and C_d are diffusion conductance and diffusion capacitance, respectively. Specifically, $g_d=(1/V_t)(I_{p0}+I_{n0})$ and $C_d=(1/2V_t)(I_{p0}\,\tau_{p0}+I_{n0}\,\tau_{n0})$.

The equivalent circuit diagram of the studied PN junction is shown in Figure 4, where dynamic compressive forces are applied. Generally, the C_d is replaced by a series of piezoelectric diffusion capacitors, i.e. C_{pd0}, C_{pd1}, C_{pd2}… It is true that all the periodic dynamic external forces applied can be expressed via Fourier expansion with each sinusoidal term leading to one-to-one corresponding diffusion capacitors. C_j is junction capacitance, r_d is resistor of the PN junction, and r_s represents the resistor of the external circuit. I_D is the external current. Based on the above analysis, the admittance Y under a dynamic force with the frequency varying in [1 Hz, 1 KHz] is numerically calculated, where g_d and C_d are approximately to be 16.8 Ω and 2.97 nF, respectively, shown in Figure 5. Figure 5 shows the admittance Y (from the equation (21))

This manuscript was accepted by J. Appl. Phys. Click here to see the version of record.

when the device is under the stress at low frequency. It illustrates how the admittance is formed by conductance g_d and diffusion capacitance C_d induced by the external stress. As Y is a complex number, we only show few points in the figure. The unit of g_d is 1/Ω. Under the small signal model, the dynamic compressive force introduces DC components c_1 and c_2 which modulate the external voltage V_{dc}, therefore changing the currents I_{n0} and I_{p0}, which are closely related to Y.

To see how the external compressive stress affects the current output, we have calculated the case when V_{dc}=1V and ω=10Hz with other parameters unchanged. The result is shown in Figure 6. It is seen that an AC output with the same frequency as the external compressive stress when there is only V_{dc} applied, which means that the external stress can modulate the current output of the device and acts as an alternating voltage source. The DC output component is indicated in Figure 6. It should be noted that this DC component is different with the one provided only by V_{dc}. In other words, the external stress not only adds the AC component but also modulates the DC component.

3.2 High Frequency

For high frequency external forces, we employ the unified approach [27] for analyzing the dynamic characteristics. When the compressive force is applied at a high frequency, the excess carrier concentration in the n region is then expected to be a more general form:

$$\delta p_n(x,t) = \sum_{k=-\infty}^{\infty} \delta p_{nk}(x)\, e^{ik\omega t} \tag{22}$$

Inserting above expression into equation (16) considering the orthogonality of harmonics, the general solutions for $\delta p_{nk}(z)$ and $\delta n_{pk}(z)$ (excess carrier concentrations of holes in n region and electrons in p region when the external voltage is applied) can be derived:

$$\delta p_{nk}(x) = C_{pk}^{+} \exp\left(-\Lambda_{pk}\frac{x-W_n}{L_p}\right) + C_{pk}^{-} \exp\left(\Lambda_{pk}\frac{x-W_n}{L_p}\right) \tag{23}$$

where C_{pk}^{+} and C_{pk}^{-} are constants for each harmonics and $\Lambda_{pk}=a_{pk}+ib_{pk}$ with:

$$a_{pk} = \frac{1}{\sqrt{2}}\sqrt{1+\sqrt{1+(k\omega\tau_p)^2}}, \quad b_{pk} = \frac{k\omega\tau_p}{2a_{pk}} \tag{24}$$

When the thickness of the neutral part of the PN junction is much larger than the width of the depletion, i.e. $d_n >> W_n$, the C_{pk}^{-} in equation (23) should be 0 so that $\mathrm{Re}\Lambda_{pk}=a_{pk}$ can be satisfied. The constant C_{pk}^{+} in equation (23) can be found by applying conventional injection boundary conditions $\delta p_{pn}(W_n, t)=p_{n0}f(t)$, in which $f(t)=\exp(qv(t)/kT)-1$ with $v(t)=p_{dc}''+v_1(t)-v_2(t)$. Then C_{pk}^{+} is given by:

$$C_{pk}^{+} = p_{n0}F_k, \; F_k = \frac{1}{2\pi}\int_{-\pi}^{\pi} f(t)e^{-ik\omega t}d\omega t \tag{25}$$

Substituting $f(t)$ into F_k, it arrives:

$$F_0 = I_0(\beta V_{\sim})\exp(\beta V_0) - 1; F_k = F_{-k} = I_k(\beta V_{\sim})\exp(\beta V_0) \tag{26}$$

where in equation (26) the modified Bessel functions have been introduced, which is defined by:

$$I_k(\beta V_{\sim}) = \frac{1}{\pi}\int_0^{\pi} e^{\beta V_{\sim}\cos\omega t}\cos k\omega t d\omega t. \tag{27}$$

In equations (26) and (27), $\beta=e/kT$, $V_{\sim}$ represents the amplitude of the time-varying signal that

This manuscript was accepted by J. Appl. Phys. Click here to see the version of record.

is created by time varied compressive stress. Taking equations (23-27) together into consideration, the $\delta p_n(x,t)$ is finally given by:

$$\delta p_n(x,t) = p_{n0} \sum_{-\infty}^{\infty} F_k \exp(-\Lambda_{pk} \frac{x-W_n}{L_p}) e^{ik\omega t} \quad (28)$$

Likewise, the excess carrier of electron in p region also can be derived, which is given by:

$$\delta n_p(x,t) = n_{p0} \sum_{-\infty}^{\infty} F_k \exp(\Lambda_{nk} \frac{x+W_n}{L_n}) e^{ik\omega t} \quad (29)$$

The current flowing through the junction is then given by:

$$\mathrm{J(t)} = -\mathrm{q}D_p \frac{\partial \delta p_n}{\partial x}\Big|_{x=W_n} A + \mathrm{q}D_n \frac{\partial \delta n_p}{\partial x}\Big|_{x=-W_p} A \quad (30)$$

Based on the reference [27], the dynamic characteristics of the PN junction, i.e. dynamic conductance g_d and diffusion capacitance C_d for the P^+N type junction are

$$g_d(\omega, V_\sim) = \frac{\sqrt{1+\sqrt{1+\omega^2\tau_p^2}}}{\sqrt{2}} \frac{I_1(\beta V_\sim)}{\beta V_{\sim/2}} g_{d0}(V_0) \quad (31)$$

$$C_d(\omega, V_\sim) = \frac{\sqrt{2}}{\sqrt{1+\sqrt{1+\omega^2\tau_p^2}}} \frac{I_1(\beta V_\sim)}{\beta V_{\sim/2}} C_{d0}(V_0) \quad (32)$$

where $g_{d0}(V_0)=2/\tau_p C_{d0}(V_0)=J_s exp(\beta V_0)/(kT/e)$. In this work, the $V_0=V_{dc}''$ and $V_\sim \approx c_3$, with c_4 assumed to be a much smaller value in our case. By setting k=0, we have DC current J_0 from equation (30). It is noted that the dynamic compressive force affects the J_0 as well as dynamic part of overall external current.

Numerically, we have investigated the DC current J_0 under compressive forces with different amplitudes, indicated by different initial piezoelectric charge width W_{pz1} shown in Figure 8, to reveal that the static current changes with the applied dynamic compressive force. As seen in Figure 8, V_{dc} is taken in the range of [0, 1.3V], however, due to the dynamic built-in potential introducing other DC voltage terms, i.e. c_1 and c_2, the actual voltage applied V_{dc}'' is changing with different compressive forces. Specifically, the J-V curve shifts due to various piezoelectrically induced depletion width.

Subsequently, we have calculated the dynamic characteristics, i.e. diffusion capacitance C_d and diffusion conductance G_d shown in Figure 9. As the C_d and G_d are closely related to the frequency (ω_p) of dynamic compressive force, we then vary the ω_p in a higher range [$1x10^7$, $1x10^{10}$] to reveal the frequency dependence of C_d and G_d. As different dynamic compressive forces cause different initial stains ε_0, it is obvious that G_d increases with ω_p and sensitive to the initial dynamic compressive strain. The C_d on the other hand decreases sharply at the lower range of ω_p and saturates as ω_p becomes higher. It is sensitive to the initial dynamic compressive strain. In contrast to the static case, we have derived the relation between the diffusion capacitance and the dynamic external stress. By analysing the diffusion capacitance, the dynamic characteristics of piezoelectric device can be obtained. The equations of the diffusion capacitance for the stresses with low and high frequencies are described respectively. For high frequency stresses, both dynamic conductance g_d and diffusion capacitance C_d vary with the

external frequency ω_p (shown in Figure 9), while they are regarded as constants under low frequency stresses.

4. Dynamic analysis of recombination process in piezotronics and piezo-phototronics

The piezopotential affects the recombination process happening in the depletion region, and the recombination process subsequently affects the carriers transportation and electron-photon interactions in piezotronics and piezo-phototronics. Therefore, understanding the mechanism of the recombination subject to the piezotronic effect is essential. In the PN junction studied in previous sections with one of its *n*-part made by the ZnO, the recombination process happening in the depletion region is mainly attributed to the defect assisted bulk and surface recombination-generation process, which is given by:

$$\mathrm{R} = \frac{C_n C_p N_t (np - n_i^2)}{C_n(n+n') + C_p(p+p')} \tag{33}$$

By taking $n=n_i exp((E_{fn}-E_{fi})/kT)$ and $p=n_i exp((E_{fi}-E_{fp})/kT)$, the recombination rate R in depletion region when the device is applied by a compressive force can be calculated. The calculation results are shown in Figure 10. It is seen that the R has a peak at the interface of PN junction, and the peak increases as the compressive strain increases. The position of the maximum R shifts slightly to the right when the compressive strain is increased. Dynamically, we have also calculated the maximum R subject to dynamic compressive force with different frequencies f (f=1 Hz and f=10 Hz) in Figure 11. When there is a dynamic compressive force with certain frequency is applied, the recombination rate R is dynamically varying with the same pattern as the applied force. The calculation provides a quantitative analyzing method on the impact on the recombination and transportation process due to the piezotronic effect.

In a typical PN junction, the total forward-bias current is the sum of recombination and the diffusion current. Therefore, different external compressive stresses will lead to the different recombination rates, and in turn modulating the total current as well as the light emitting intensity in piezotronic LEDs. For illustrating on how the dynamic compressive force modulates the light emitting intensity in piezotronic LEDs, we have conducted the following analysis.

As shown in Figure 7, we treat the dotted box as the active region in which light emitting and recombination are happening and related. In this region, the rate equation of carriers (holes) can be modeled as[29,30]:

$$\frac{dp}{dt} = \frac{\eta_i I}{eV_a} - \left[A(p-p_i) + B\left(p^2 - p_i^2\right) + Cp\left(p^2 - p_i^2\right)\right] \tag{34}$$

where A is coefficient of defect assisted recombination. B and C are the coefficients of radiative recombination-generation and Auger recombination, respectively. p_i is intrinsic electron concentration. η_i is the fraction of the total current that is due to the recombination in the active region. V_a is the volume of the active region. I is the total current flowing through the external circuit in forward bias direction. Taking the parameters as: A=1x10^7, B=1x10^{-9}, C=5x10^{-29}, N_A=1x10^{17}/cm^3, N_D=1x10^{15}/cm^3, initial piezoelectric stain ε_0=0.02/100, and by fixing I=0.1 A, we have calculated the number of photons emitted per second in V_a. The result is shown in Figure 12, where six different frequencies of dynamic compressive forces are studied. The light emitting in piezotronics devices is closely related to the dynamic force applied.

Conclusion

To conclude, dynamic built-in potential is induced in the piezotronic PN junction when a dynamic compressive stress is applied. The dynamic built-in potential contributes both DC and AC parts together with the applied external voltage, which can modulate current-voltage characteristics, threshold, diffusion capacitance and conductance. The work has thoroughly investigated these dynamic characteristics under external compressive stresses at both low and high frequencies based on the small signal model and unified approach, respectively. The results are self-consistent and provide a general procedure for treating dynamic phenomenon of piezotronics. The piezotronic PN junction is the fundamental element of the piezo-phototronic LEDs. The work has quantitatively calculated the dynamic recombination rate and light emitting intensity. Unlike the previous work, this work presents detailed results assisting in understanding how the piezo-potential affects the dynamic process of carriers in the piezo-phototronic LEDs.

References

1. Z. L. Wang and W. Z. Wu, Natl Sci Rev 1 (1), 62-90 (2014).
2. Z. L. Wang and J. H. Song, Science 312 (5771), 242-246 (2006).
3. W. Z. Wu, L. Wang, Y. L. Li, F. Zhang, L. Lin, S. M. Niu, D. Chenet, X. Zhang, Y. F. Hao, T. F. Heinz, J. Hone and Z. L. Wang, Nature 514 (7523), 470-+ (2014).
4. Z. L. Wang, Nano Today 5 (6), 540-552 (2010).
5. M. Z. Peng, Z. Li, C. H. Liu, Q. Zheng, X. Q. Shi, M. Song, Y. Zhang, S. Y. Du, J. Y. Zhai and Z. L. Wang, Acs Nano 9 (3), 3143-3150 (2015).
6. R. R. Bao, C. F. Wang, L. Dong, R. M. Yu, K. Zhao, Z. L. Wang and C. F. Pan, Adv Funct Mater 25 (19), 2884-2891 (2015).
7. Y. Liu, Q. Yang, Y. Zhang, Z. Y. Yang and Z. L. Wang, Adv Mater 24 (11), 1410-1417 (2012).
8. Y. Dai, X. Wang, W. Peng, H. Zou, R. Yu, Y. Ding, C. Wu and Z. L. Wang, ACS Nano 11 (7), 7118-7125 (2017).
9. Z. Zhang, Q. Liao, Y. Yu, X. Wang and Y. Zhang, Nano Energy 9, 237-244 (2014).
10. C. F. Pan, S. M. Niu, Y. Ding, L. Dong, R. M. Yu, Y. Liu, G. Zhu and Z. L. Wang, Nano Lett 12 (6), 3302-3307 (2012).
11. L. Zhu, L. Wang, F. Xue, L. Chen, J. Fu, X. Feng, T. Li and Z. L. Wang, Advanced Science 4 (1), 1600185 (2017).
12. Y. Zhang, Y. Yang, Y. Gu, X. Yan, Q. Liao, P. Li, Z. Zhang and Z. Wang, Nano Energy 14 (Supplement C), 30-48 (2015).
13. P. Bonato, Ieee Eng Med Biol 29 (3), 25-36 (2010).
14. W. Wu and Z. L. Wang, NATURE REVIEWS MATERIALS 1 (16031), 1-17 (2016).
15. D. H. Kim, Science 333 (6050), 1703-1703 (2011).
16. X. Wang, M. Que, M. Chen, X. Han, X. Li, C. Pan and Z. L. Wang, Advanced Materials 29 (15), 1605817 (2017).
17. Y. Zhang, X. Yan, Y. Yang, Y. Huang, Q. Liao and J. Qi, Advanced Materials 24 (34), 4647-4655 (2012).
18. Y. Zhang, Y. Liu and Z. L. Wang, Adv Mater 23 (27), 3004-3013 (2011).
19. W. Liu, A. H. Zhang, Y. Zhang and Z. L. Wang, Nano Energy 14, 355-363 (2015).

20. L. S. Jin and L. J. Li, Nano Energy 15, 776-781 (2015).
21. W. Liu, A. H. Zhang, Y. Zhang and Z. L. Wang, Appl Phys Lett 107 (8) (2015).
22. A. Rinaldi, R. Araneo, S. Celozzi, M. Pea and A. Notargiacomo, Adv Mater 26 (34), 5976-+ (2014).
23. M. X. Chen, C. F. Pan, T. P. Zhang, X. Y. Li, R. R. Liang and Z. L. Wang, Acs Nano 10 (6), 6074-6079 (2016).
24. Z. N. Wang, R. M. Yu, X. F. Wang, W. Z. Wu and Z. L. Wang, Adv Mater 28 (32), 6880-+ (2016).
25. S. Kim, J. Ha and J. B. Kim, J Comput Electron 15 (1), 40-44 (2016).
26. X. Y. Li, M. X. Chen, R. M. Yu, T. P. Zhang, D. S. Song, R. R. Liang, Q. L. Zhang, S. B. Cheng, L. Dong, A. L. Pan, Z. L. Wang, J. Zhu and C. F. Pan, Adv Mater 27 (30), 4447-4453 (2015).
27. A. A. Barybin and E. J. P. Santos, Semicond Sci Tech 22 (11), 1225-1231 (2007).
28. Y. Liu, S. Niu, Q. Yang, B. D. B. Klein, Y. S. Zhou and Z. L. Wang, Advanced Materials 26 (42), 7209-7216 (2014).
29. J. Singh, *Electronic and Optoelectronic Properties of Semiconductor Structures* (Springer Netherlands, 2008).
30. N. P. SL Chuang, S Koch,, *Physics of Optoelectronic Devices*. (Wiley, 2008).

Acknowledgements

National Natural Science Foundation of China (61604078), Natural Science Youth Foundation of Jiangsu Province (BK20160905). Natural Science Foundation of the Jiangsu Higher Education Institutions of China (16KJB510029), Postdoctoral Science Foundation of China and Jiangsu Province (2017M610341, 1701044A), Jiangsu Natural Science Foundation for Excellent Young Scholar (BK20170101) and NUPTSF (NY216010) are acknowledged. SPARC II (Solar Photovoltaic Academic Research Consortium) project funded by the Welsh European Funding Office is acknowledged.

Additional information

Competing financial interests: The authors declare no competing financial interests.

Figure Captions:

Figure 1. Schematic diagram of the piezotronics effect: a typical PN junction with N part made by ZnO.

Figure 2. Calculation of dynamic built-in potential when there is a dynamic compressed force applied with frequency ω_p=1 KHz.

Figure 3. Energy bands of the studied PN junction under different strains. From red to green, strains are 0.002, 0.005, 0.008 and 0.01.

Figure 4. General equivalent circuit diagram of the studied PN Junction under small signal assumption.

Figure 5. Admittance calculation when the device is under an external compressed

force with frequency varying in [1 Hz, 1 KHz]

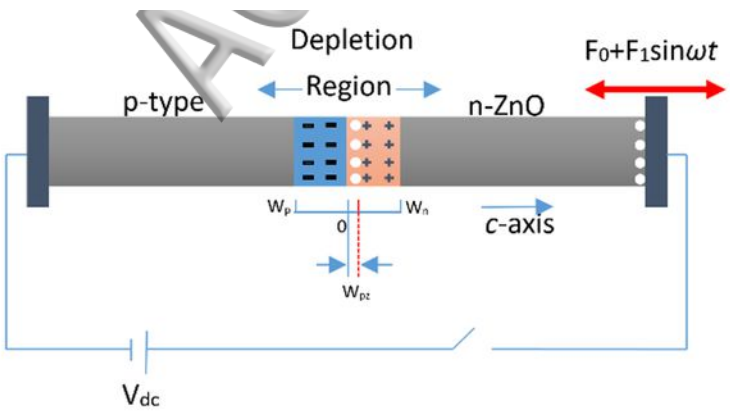
Depletion
Region
p-type
n-ZnO
F0+F1sinωt
Wp
Wn
0
c-axis
Wpz
Vdc

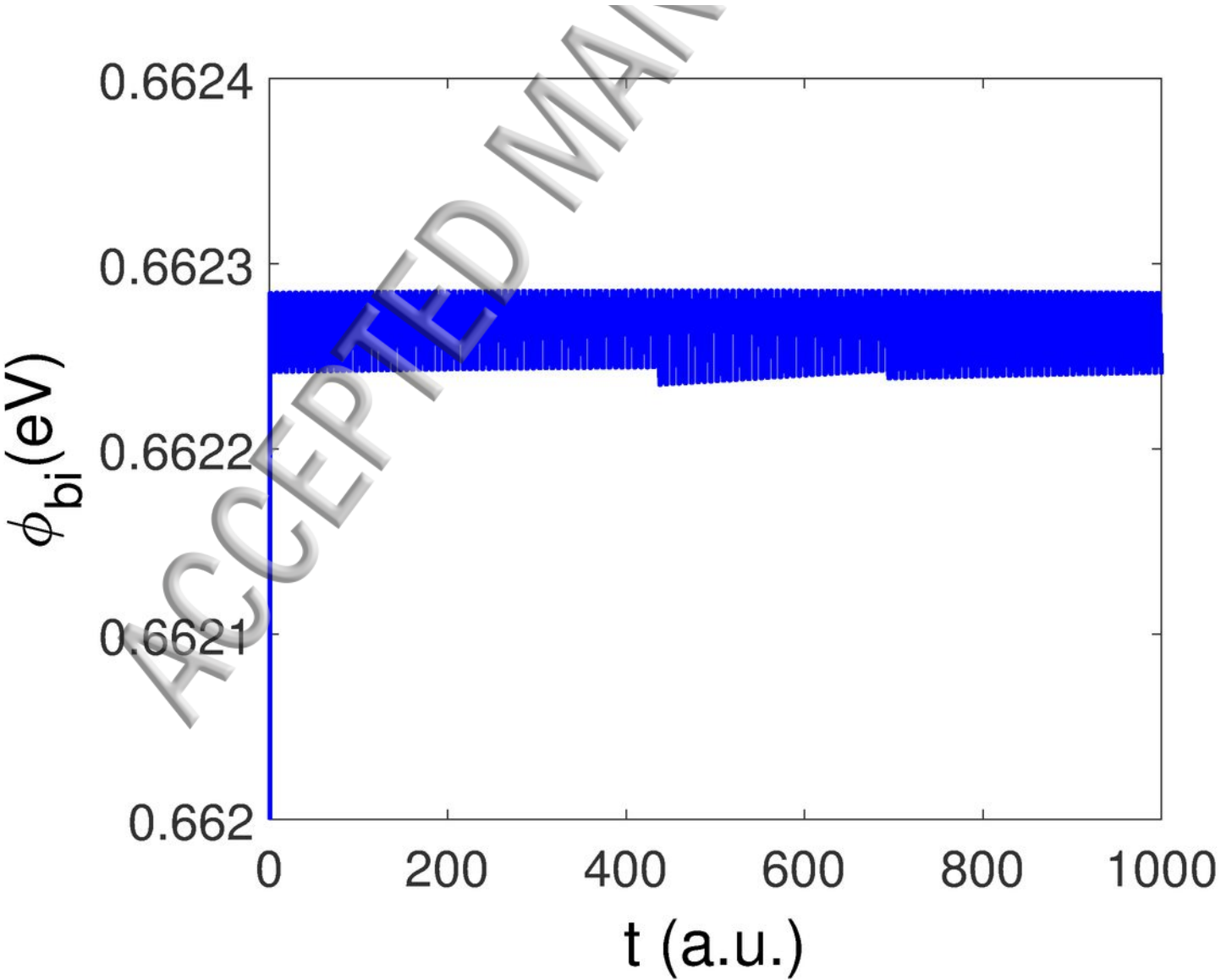

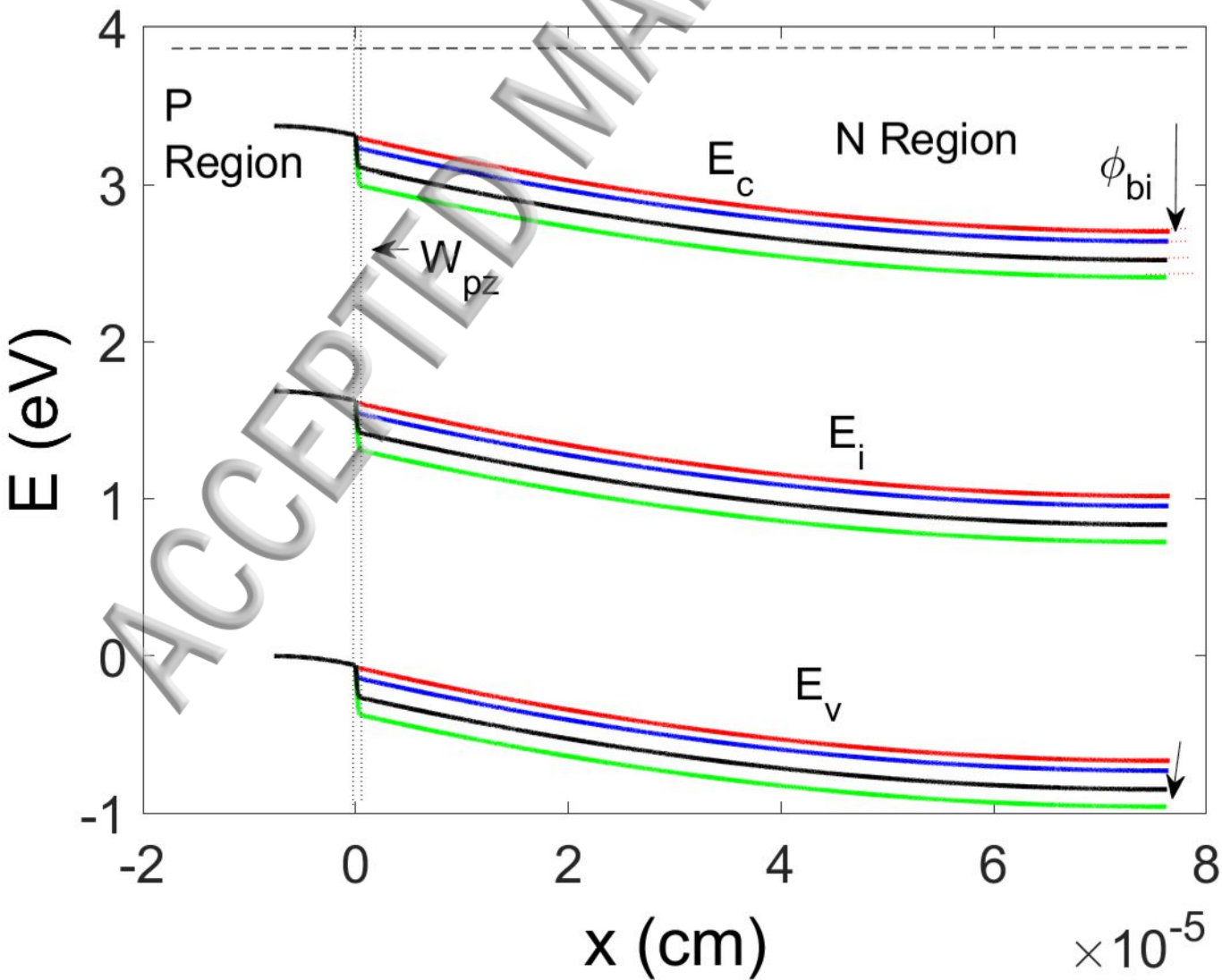

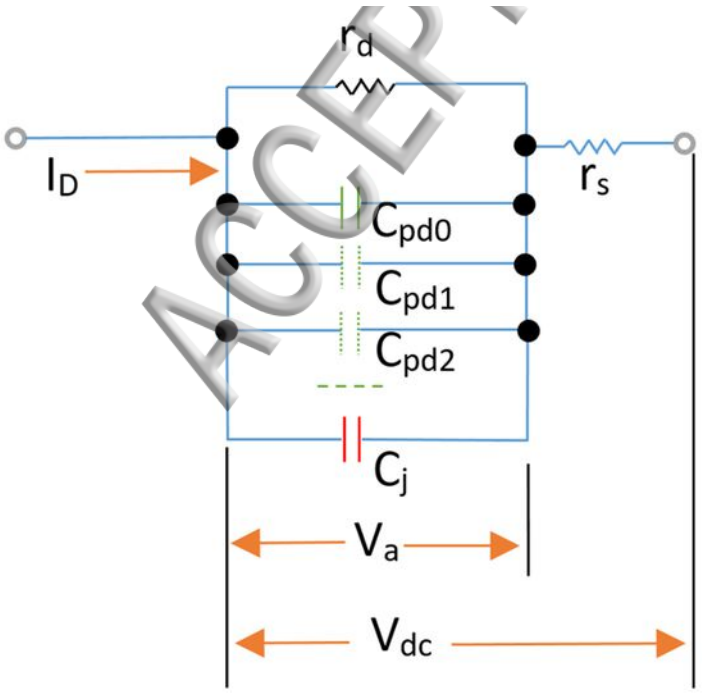
r_d
I_D
r_s
C_{pd0}
C_{pd1}
C_{pd2}
C_j
V_a
V_{dc}

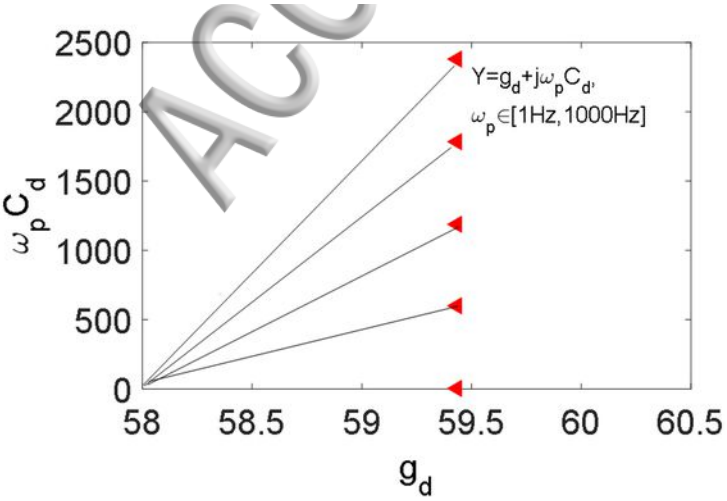
2500
2000
1500
1000
500
0
58
58.5
59
59.5
60
60.5
$\omega_p C_d$
g_d
$Y=g_d+j\omega_p C_d$,
$\omega_p \in [1Hz, 1000Hz]$

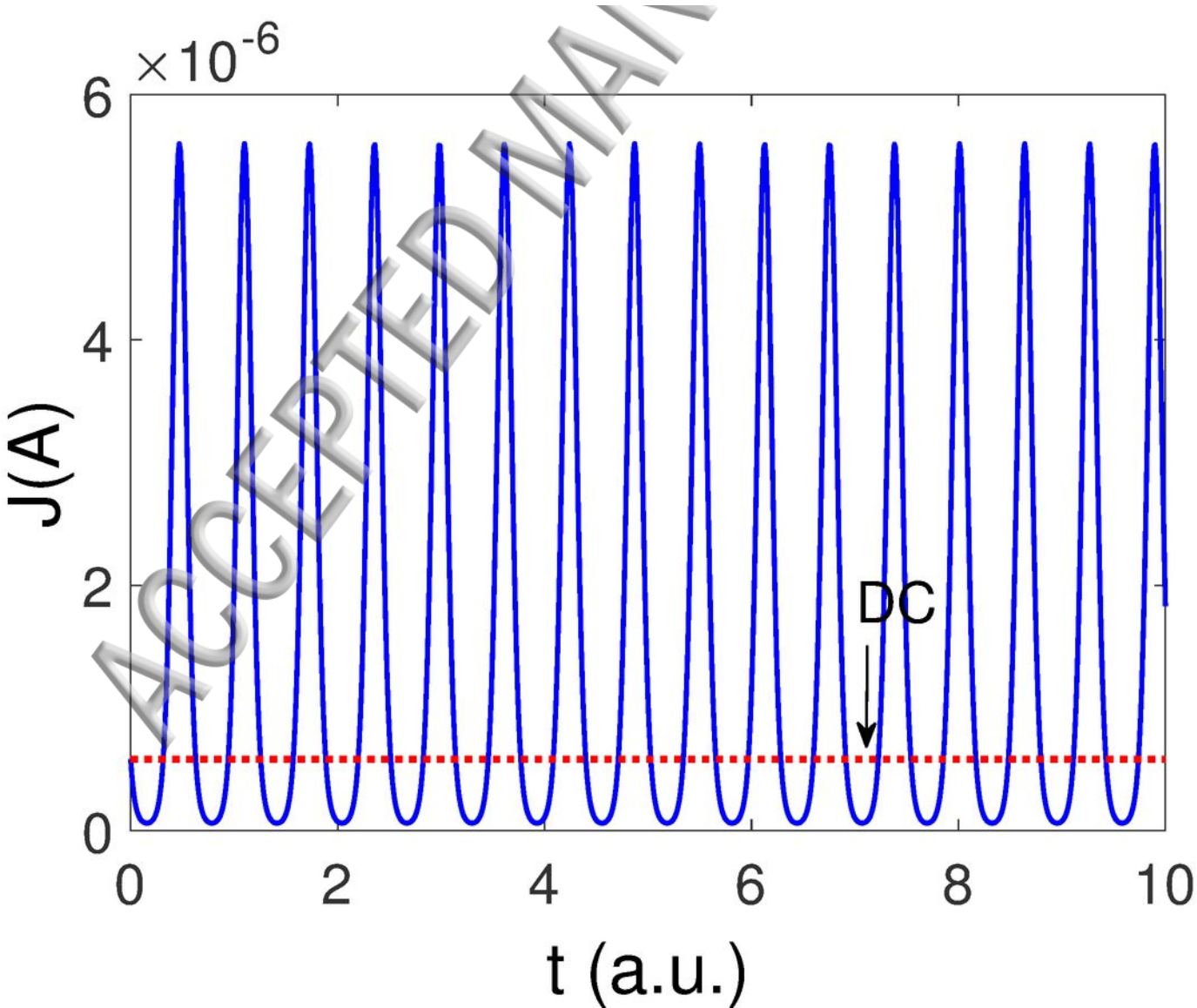

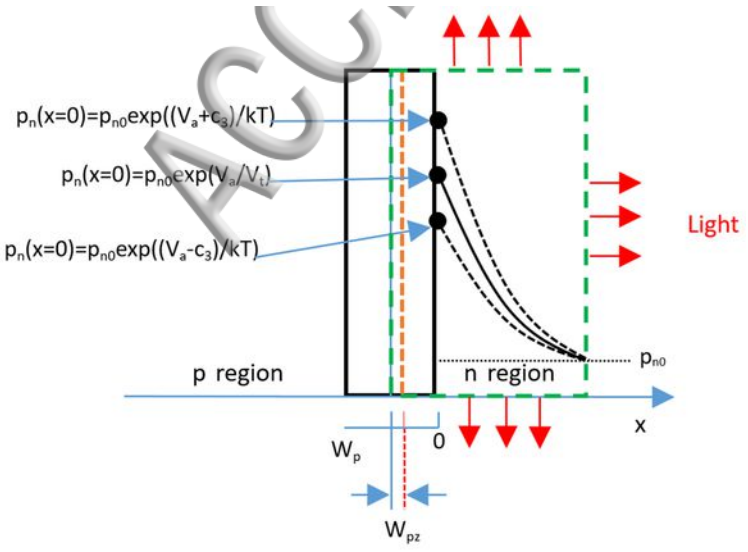
$p_n(x=0)=p_{n0}\exp((V_a+c_3)/kT)$
$p_n(x=0)=p_{n0}\exp(V_a/V_t)$
$p_n(x=0)=p_{n0}\exp((V_a-c_3)/kT)$
Light
p_{n0}
p region
n region
x
0
W_p
W_{pz}

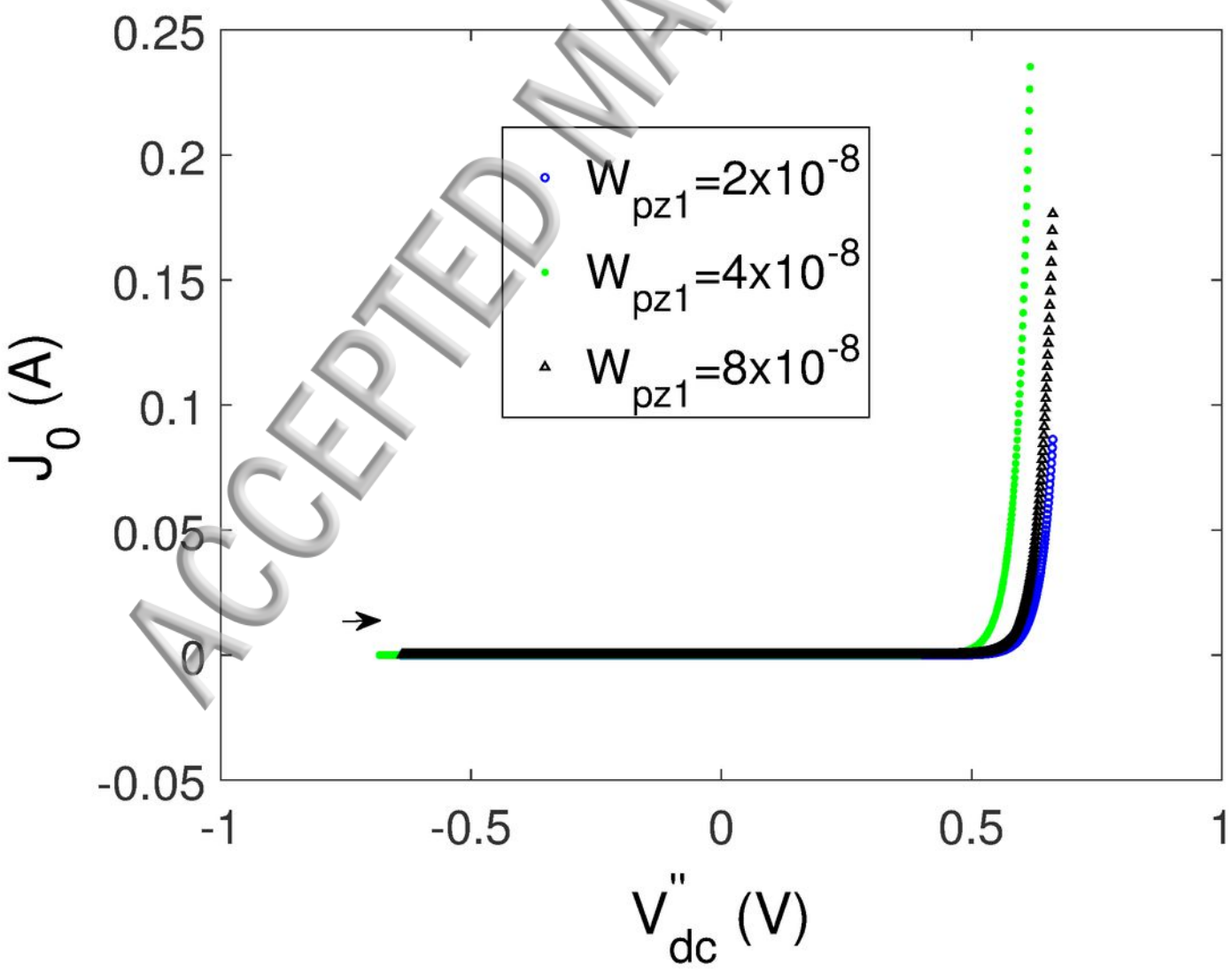

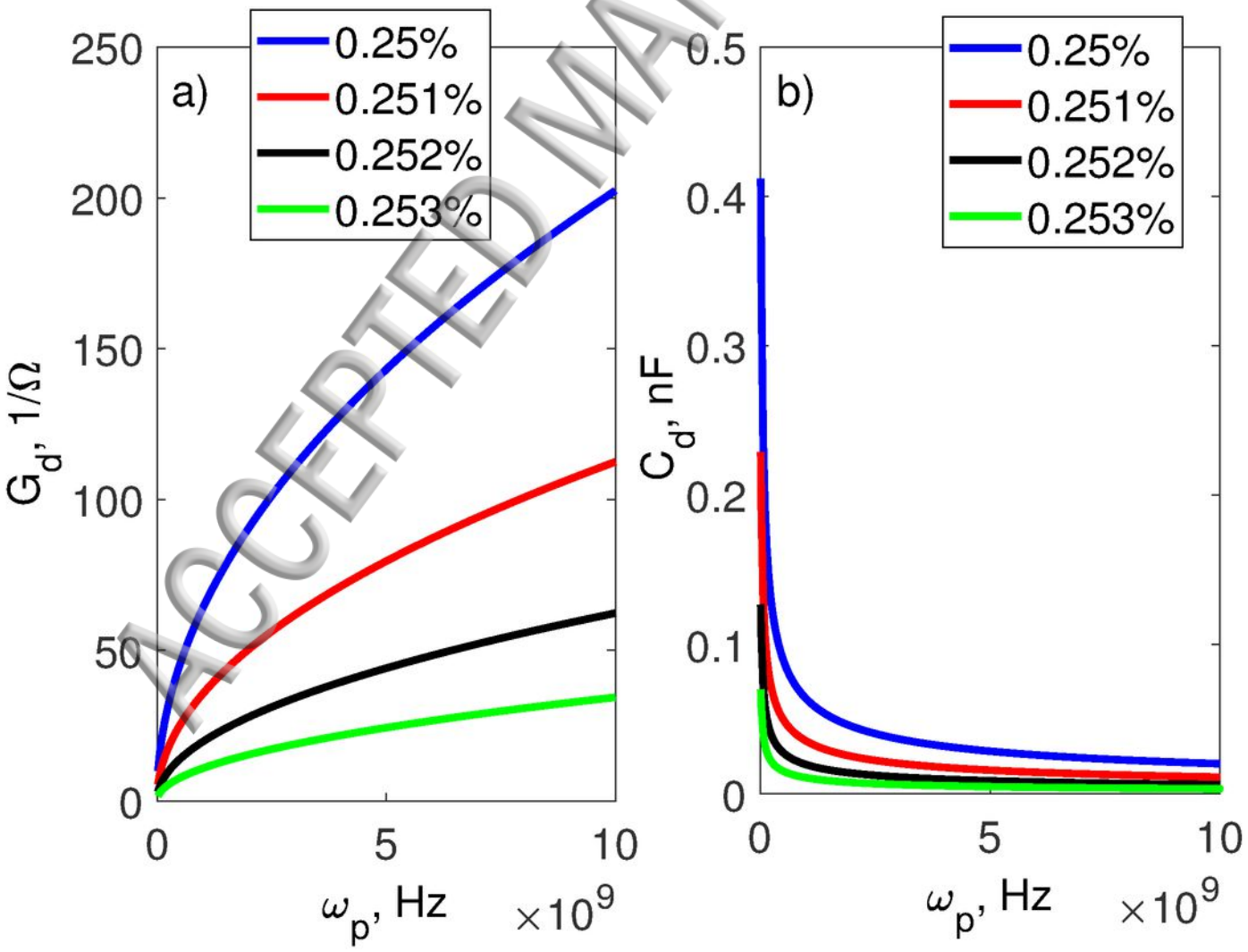

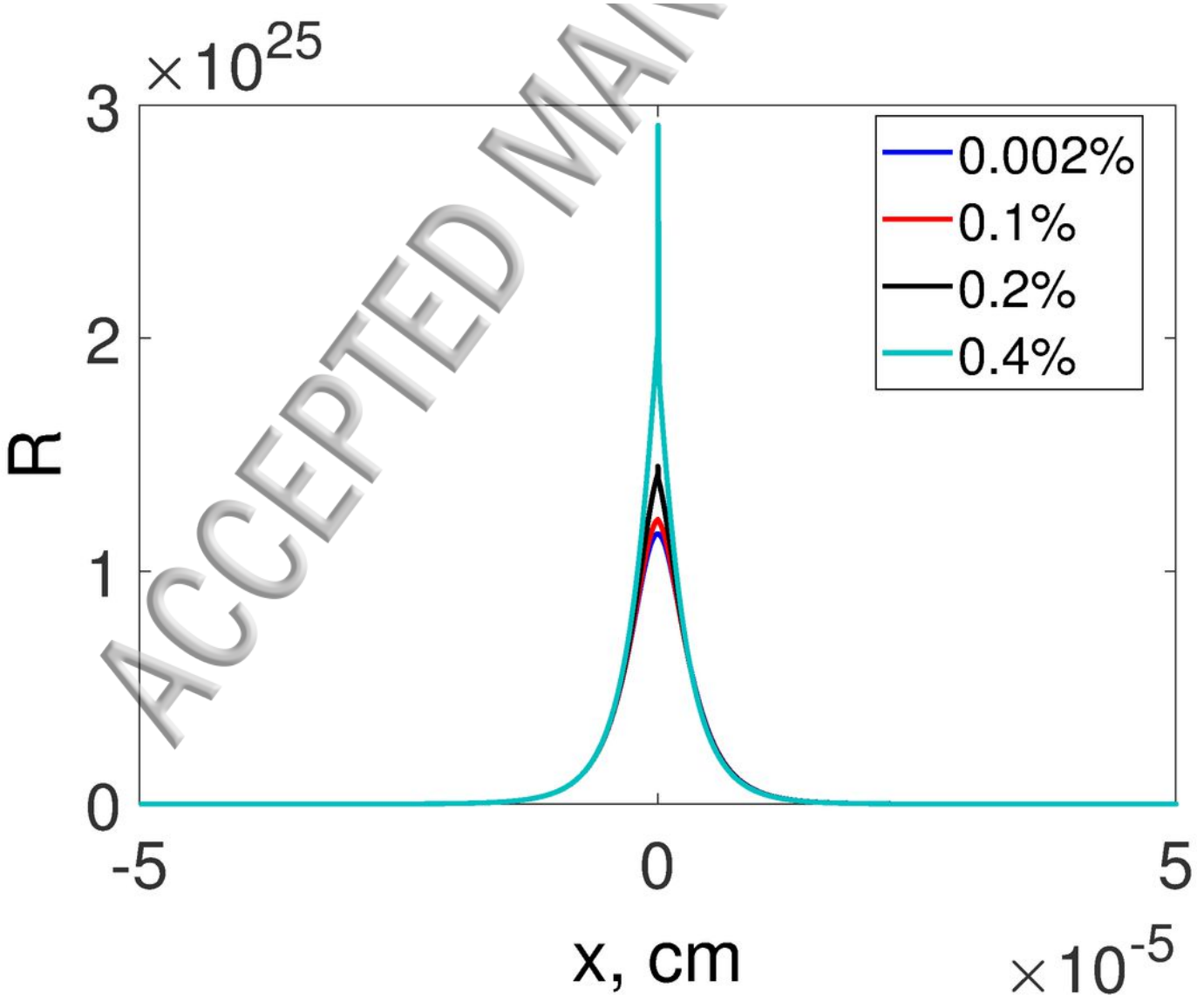

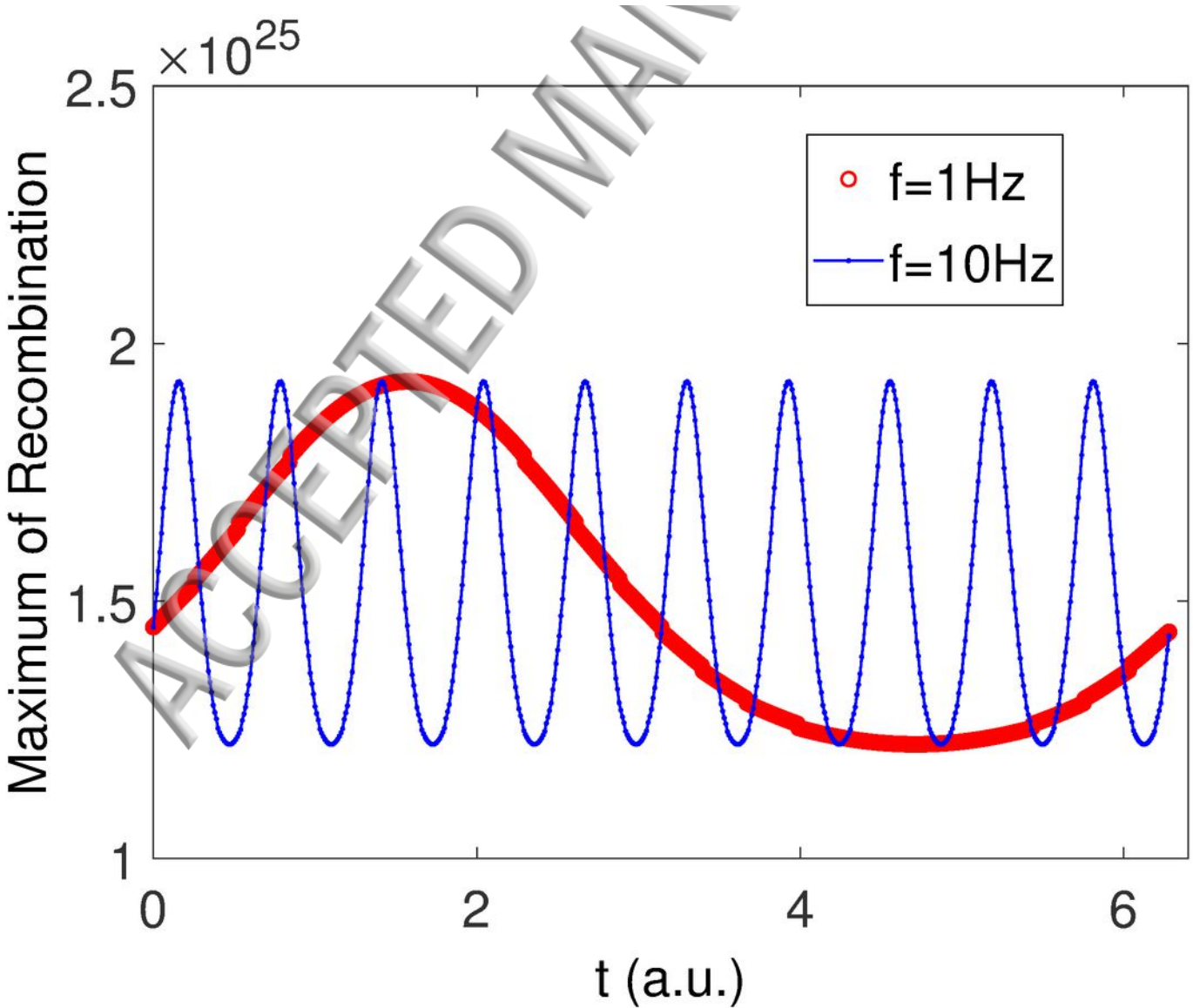

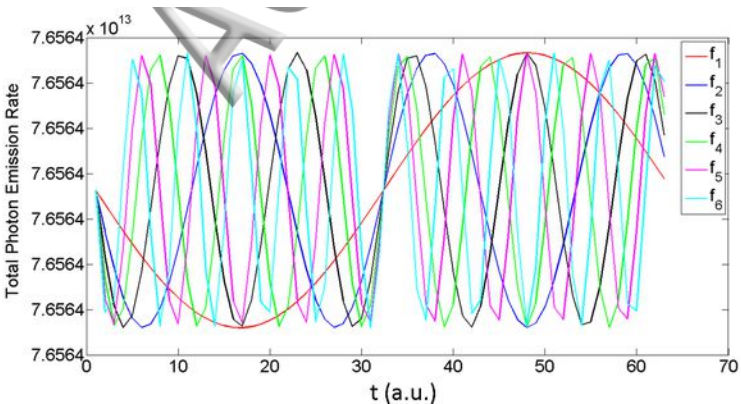
x 10^13
7.6564
7.6564
7.6564
7.6564
7.6564
7.6564
7.6564
Total Photon Emission Rate
0
10
20
30
40
50
60
70
t (a.u.)
f1
f2
f3
f4
f5
f6